Applied Thermal Engineering 130 (2018) 1256–1265

Contents lists available at ScienceDirect

Applied Thermal Engineering

journal homepage: www.elsevier.com/locate/apthermeng

Research Paper

Numerical prediction of velocity coefficient for a radial-inflow turbine stator using R123 as working fluid

Bensi Dong [a], Guoqiang Xu [a], Tingting Li [b], Yongkai Quan [a], Lijing Zhai [a], Jie Wen [a,*]

[a] National Key Laboratory of Science and Technology on Aero-thermodynamics, School of Energy and Power Engineering, Beihang University, Beijing 100191, China
[b] Department of Mechanical Engineering, Texas A&M University, College Station, TX 77843-3123, United States

HIGHLIGHTS

- The velocity coefficient for the stator using R123 is investigated numerically.
- The effects of five key parameters on the velocity coefficient are evaluated.
- A model considering surface roughness is derived for high Reynolds number condition.
- The potentially wide application of the modified model is preliminary confirmed.

ARTICLE INFO

Article history:
Received 30 June 2017
Revised 30 October 2017
Accepted 12 November 2017
Available online 13 November 2017

Keywords:
Organic Rankine cycle
Radial turbine stator
Velocity coefficient
Refrigerant
Computational fluid dynamics

ABSTRACT

Organic Rankine cycle (ORC) is a reliable technology for converting low-grade heat into electricity. The accurate design of its expander is the key to ensure an expected cycle efficiency. This work numerically investigates the stator velocity coefficient for the radial ORC turbine using R123 as working fluid. The effects of outlet blade angle, solidity, blade height, expansion ratio, and surface roughness, on the stator velocity coefficient are evaluated by a verified 3-D viscous numerical modeling. A modified 1-D model is also derived within a wide range of various parameters. The results show that the velocity coefficient is relatively sensitive to both blade height and surface roughness while almost independent of expansion ratio, mainly due to the high Reynolds number and the small flow boundary layer when using refrigerant vapor. Since the existing semi-empirical formula fails to well capture the velocity coefficient for the stator with rough wall, a modified model considering the surface roughness successfully resolve this issue with a maximum deviation around 3.5%. Its applicability for the stators with different stator inlet conditions (380–410 K) and working fluid (R245fa) is further explored, and the results also exhibits satisfactory accuracy.

1. Introduction

In recent years, organic Rankine cycle (ORC) has attracted considerable attention due to the growing interest in converting low-grade thermal energy into electricity. Current applications of ORC system are mainly for the power generation using renewable energy (e.g. geothermal resource [1], biomass [2], solar [3]) and waste heat energy [4] as the heat sources. The superiorities of ORC over other low-grade thermodynamic cycles include higher efficiency, smaller size, higher reliability, and lower emission [5]. Nevertheless, the cycle efficiency of ORC remains at a low level due to the relatively low operating temperature. Therefore, the design of a high-performance ORC expander, which mainly limits the ORC system efficiency, becomes particularly critical.

Generally, typical expanders can be classified into two categories: one is the volume expander, applicable for the ORC system with small scale and low expansion ratio, such as scroll expander [6], screw expander [7], and rotary expander [8]; the other one is the velocity expander (known as turbine), including axial turbine and radial turbine, which is appropriate for use in large-sized commercial ORC system. Due to the characteristics of low mass flow rate and high expansion ratio for a typical commercial ORC, radial turbine is a better option for ORC systems, following the reasons below: (1) It has the capacity to deal with large enthalpy drop at the low peripheral; (2) It is less sensitive to blade profile inaccuracies; (3) It can maintain a high efficiency at off-design working conditions; (4) Its rotor shows higher dynamic stability; (5) Its sealing structure is simpler [9].

* Corresponding author.
E-mail address: wenjie@buaa.edu.cn (J. Wen).

https://doi.org/10.1016/j.applthermaleng.2017.11.063
1359-4311/

Nomenclature

P	pressure [kPa]
T	temperature [K]
v	specific volume [m^3/kg]
h	specific enthalpy [kJ/kg]
c	absolute velocity [m/s]
E	energy factor
C	loss coefficient multiplier
l	surface length [m]
Re	Reynolds number
s	blade spacing at blade-row exit [m]
A	area [m^2]
t	trailing-edge thickness [m]
H	form factor
b	chord [m]
d	blade height [m] or outlet diameter [m]
R_x	surface roughness [μm]
k	specific heat ratio
c_p	specific heat at constant pressure [kJ/kg·K]
c_v	specific heat at constant volume [kJ/kg·K]
m	mass flow rate [kg/s]
r	radius [m]
q	heat loss [kJ]

Greek symbols

ω	acentric factor
φ	stator velocity coefficient
ζ	stator loss
θ	momentum thickness
γ	flow angle from throughflow direction [°]
α	outlet blade angle [°]
π	expansion ratio
ρ	density [kg/m^3]
μ	dynamic viscosity [Pa·s]
θ_{cam}	camber angle [°]

Subscripts

cr	critical
0	inlet
1	outlet
s	isentropic
n	stator
tot	total
ref	reference
f	fit
b	blade
w	endwall

Although conventional radial turbine is less investigated compared to the axial one, its design methods are also quite mature, most of which are based on the studies performed by NASA Lewis Research Center [10]. However, due to the significant differences in the physical properties between organic fluids and conventional working fluids (gas and steam), the ORC radial turbine shows some distinguished characteristics: (1) Large molecular weight (low sound speed) contributes to a high Mach number at the stator outlet; (2) High density leads to a small size and therefore a high shaft speed; (3) A low enthalpy drop occurs with a high expansion ratio. As the expansion process is close to the saturation vapor curve and also the critical point, using the ideal gas equation for conventional turbine design is not applicable to the radial ORC turbine design. Based on these characteristics, some modeling and experimental studies on the radial ORC turbine have been performed. Fiaschi et al. [10] developed a 0-D model for a small-size radial ORC turbine to investigate the behavior of turbine performance against several main design parameters. Rahbar et al. [11] adopted genetic algorithm to optimize the performance of radial ORC turbine within a wide range of geometrical and operating parameters. Song et al. [12], Pan and Wang [13], and Pezzuolo et al. [14] coupled the thermodynamic analysis of ORC system with a preliminary design model of radial turbine to explore the effect of turbine efficiency on the cycle performance. According to the results from the preliminary design, the design accuracy of ORC turbine can be further improved by taking advantage of the maturity of computational fluid dynamics (CFD) simulation technology. Hoffren et al. [15] and Harinck et al. [16] simulated the flow field in the stator of radial ORC turbine by utilizing 2-D CFD method. Boncinelli et al. [17] first employed 3-D numerical simulation to the rotor of a radial ORC turbine using R134a as working fluid. Harinck et al. [18] extended the steady-state 3-D CFD method to the entire radial ORC turbine. Recently, due to the popularity of the commercial CFD software, great interest has been aroused in research on numerical simulation of radial ORC turbine. Sauret and Gu [19] first presented the whole design process of the candidate R143a radial turbine in the application of geothermal energy and carried out the simulations of radial ORC turbine under the nominal and off-design conditions. Li and Ren [20] developed an aerodynamic and profile design system for a 500 kW radial turbine with R123 as working fluid. Afterwards, the same research team established an optimization framework for the nozzle, meridional flow path, and blade profile with the combination of CFD software [21]. Jubori et al. [22] numerically investigated the performance of micro-scale radial turbine with different working fluids (R141b, R245fa and n-pentane) and different operating conditions. The results showed that using n-pentane achieves the highest isentropic efficiency. They also adopted CFD method to compare the performances of axial ORC turbine and radial ORC turbine, and the maximum total-to-total efficiency of radial one was slightly higher [23]. Besides, Fiaschi et al. [24], Hamdi et al. [25], and Dong et al. [26] also performed the 3-D CFD simulation for the radial ORC turbine under the different conditions of operating parameters and working fluids. In addition to the numerical studies, Kang [27,28], Li et al. [29], Inoue et al. [30], and Ludovic et al. [31] respectively conducted the experimental investigations regarding the radial turbine used in ORC system. The measured isentropic efficiencies of these radial turbines were mostly below the design values. This is possible largely due to the restriction on the experimental conditions or the use of the incorporated loss models in the preliminary design which were developed for the radial turbine operating with the ideal gas.

The preliminary design is the foundation of the entire turbine design process, as it initially determines the basic geometry, velocity triangles, and the efficiency of the designed turbine. In the calculation of different losses, the stator loss is relatively low compared to the rotor loss and often evaluated with less accuracy [10]. Compared with the isentropic flow, there exist various flow losses for the actual flow process in the stator. For simplicity in the stator design, the stator losses are usually reflected by velocity coefficient φ, defined as the ratio of the actual outlet velocity c_1 and the ideal outlet velocity c_{1s}:

$$\varphi = c_1/c_{1s} \quad (1)$$

here, φ is influenced by many factors such as structural dimensions, blade shape, machining quality, and flow parameters. In the preliminary design for an ORC turbine, φ is usually selected within the recommended range (e.g. 0.92–0.98 [32]), which is generally based on the experimental data of the conventional gas turbine. Due to the diverse physical properties for the organic vapor, adopting conventional φ may cause a great deviation in the ORC turbine design.

This work focuses on the stator of a R123 radial turbine used in a low-grade ORC system. The 3-D CFD simulations are conducted to investigate the effects of outlet blade angle, solidity, blade height, expansion ratio, and surface roughness on the stator velocity coefficient. Upon the existing prediction model, a modified model for velocity coefficient considering the surface roughness is proposed for the stator using R123, and its applicability to other operating conditions and refrigerants is discussed preliminarily as well.

The whole paper is organized as below. After this introduction section, the numerical model and method are presented in Section 2, including 3-D CFD analysis and 1-D predication model. Section 3 describes the influences on velocity coefficient under various key parameters. Then, the modified prediction model is given in Section 4, which also discusses the influence mechanism of the working fluid on velocity coefficient and the effect of the new model on the cycle's performance. Finally, Section 5 draws the research conclusions and provides the related research prospects.

2. Numerical model and method

Due to the relatively low sound speed for the organic working fluid, radial ORC turbine often operates with supersonic flow at the stator outlet. Therefore, the transonic cascade TC-4P is usually employed for the stator with relatively high expansion ratio. Although the flow channel of TC-4P is convergent, because of the oblique exit section, it shows satisfactory aerodynamic performance under the transonic condition. As such, TC-4P is selected as the blade profile for the radial ORC turbine stator [20], and its relative coordinates are shown in Table 1.

Fig. 1 summarized the flowchart of modeling, meshing, and simulation, which are conducted in UGNX 8.0, TurboGrid 15.0, and CFX 15.0, respectively. After building the geometry model, the O-H hexahedron structured computational mesh is then generated by TurboGrid 15.0 (see Fig. 2), in which local mesh refinement is implemented in the complex flow area, including the near wall area (boundary layer effect), trailing edge (trailing edge effect), and suction surface near the trailing edge (expansion wave). The mesh independence analysis is conducted by changing the element number and monitoring the mass flow rate and outlet Mach number. Fig. 3 shows the results of the mesh independence analysis for the stator with 5 mm in blade height, 1.5 in solidity, and 15° in blade outlet angle. The mesh independent result can be reached when the mesh number exceeds 1,000,000, as the changes of the key outputs are lower than 0.01%. The same mesh sensitivity analysis method is also applied to other stator structures, and the selected mesh number is proven to be sufficient enough for each geometry structure.

The commercial CFD software ANSYS-CFX 15.0 is used to perform the steady-state viscous turbulent simulation. The Navier–Stokes equations are discretized using the first order upwind advection scheme. The k-ω based shear stress transport (SST) turbulence model is adopted due to capabilities of automatic treatment for the first node near the wall to captures the turbulence closure and accurate predication on the separated flows [22,26]. The equations of state (EoS) of Soave–Redlich–Kwong (SRK) were chosen to describe the thermodynamic properties of the refrigerant R123 vapor. Its equations are presented as follows:

$$P = \frac{RT}{v-b} - \frac{a}{v}\frac{\alpha(T)}{(v+b)} \quad (2)$$

where

$$a = \frac{0.42748R^2T_{cr}^2}{P_{cr}} \quad (3)$$

$$b = \frac{0.08664RT_{cr}}{P_{cr}} \quad (4)$$

$$\alpha(T) = \left(1 + \alpha_{SRK}\left(1 - \sqrt{\frac{T}{T_{cr}}}\right)\right)^2 \quad (5)$$

$$\alpha_{SRK} = 0.48 + 1.574\omega - 0.176\omega^2 \quad (6)$$

The basic properties of R123 is presented in Table 2, including the thermodynamic properties that are obtained from the NIST database and the environmental parameters. Besides the above equations, the zero pressure specific heat capacity at constant pressure (c_{p0}) is needed to access other thermophysical properties such as specific heat, specific enthalpy, specific entropy, and sound speed. The data of c_{p0} are obtained via NIST database as well and fitted into the following fourth order polynomial:

$$c_{p0}/R = 2.996 + 0.03949T - 2.743e-05T^2 - 1.22e-09T^3 + 5.72e-12T^4 \quad (7)$$

Listed are critical pressure, critical temperature, molar mass, normal boiling temperature, acentric factor, ozone depletion potential, and global warming potential.

To determine the boundary conditions, a thermodynamic model for a basic ORC system is built with MATLAB R2013a. The turbine inlet temperature is fixed to 400 K which is 20 K below the heat source temperature of 420 K, while the corresponding pressure is set at 1200 kPa, slightly lower than saturation pressure. The condensing temperature and the associated pressure are set to be 318 K and 180.02 kPa, respectively. Given that the ambient temperature is 303 K, a 15 K pinch point temperature is produced.

Table 1
The relative coordinates of TC-4P stator.

x	0	2.5	5	7.5	10	12.5	15	17.5	20	25
y_t	0.453	1.57	2.545	3.445	4.46	5.45	6.52	7.59	8.66	10.84
y_a	0.453	0.28	0.815	1.45	2.1	2.72	3.39	4.005	4.65	5.94
x	30	35	40	45	50	55	60	65	70	75
y_t	13.06	15.35	17.69	19.9	22.4	24.4	26.35	27.7	28.6	29
y_a	7.2	8.47	9.6	10.5	11.23	11.7	12.96	11.8	10.9	9.24
x	80	82.5	85	87.5	90	92.5	95	97.5	100	
y_t	28.4	27.9	27.2	26.3	25	23.4	21.2	17.4	7.43	
y_a	7.15	5.9	4.44	2.72	0.127	0.362	0	0.905	7.43	

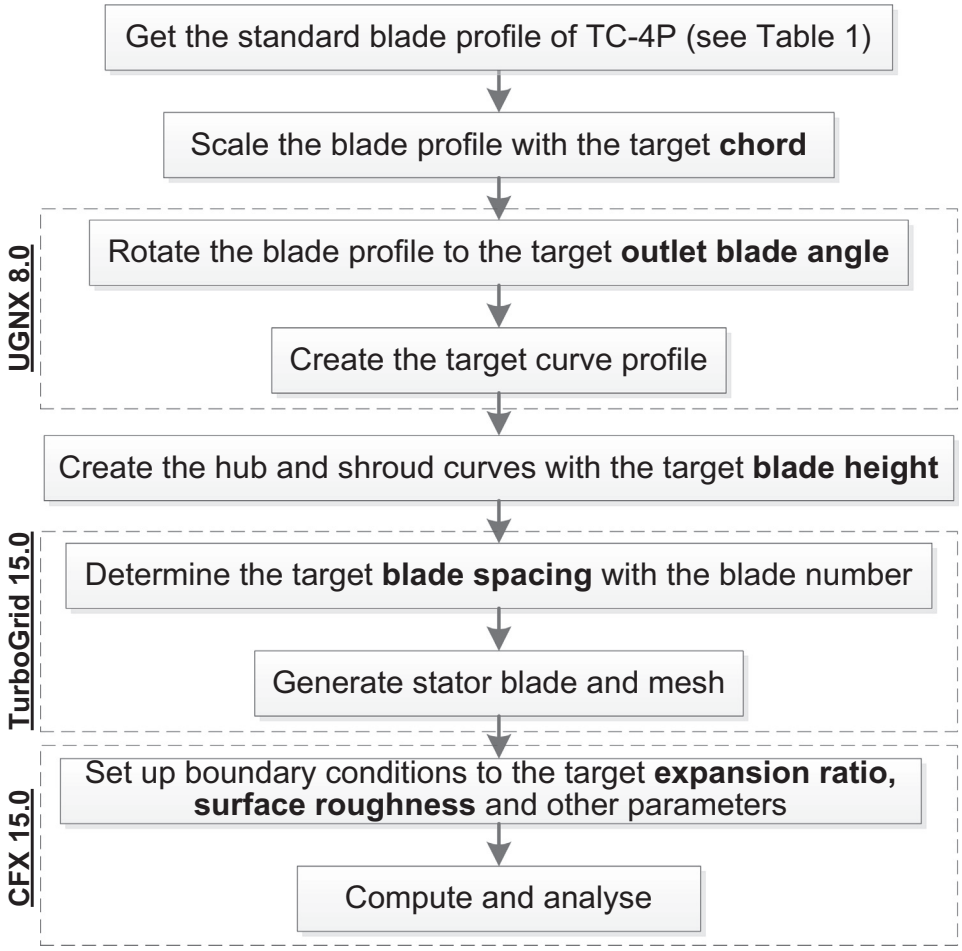

Fig. 1. Flowchart for the CFD analysis.

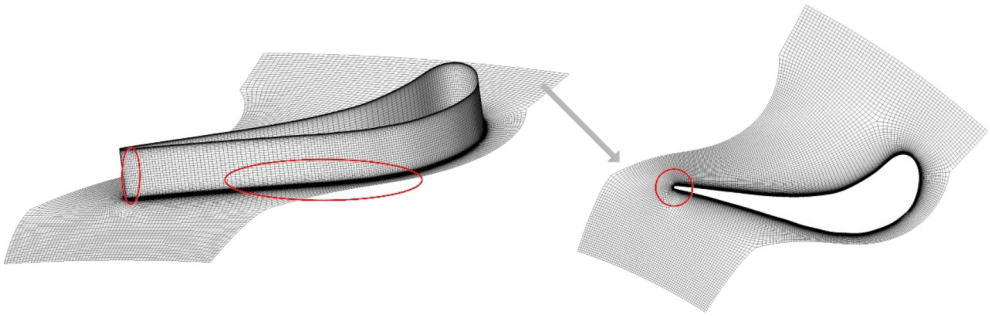

Fig. 2. The O-H mesh around the stator blade.

The boundary conditions are then defined based on the above analysis. The total pressure of 1200 kPa, total temperature of 400 K, and 5% turbulence intensity are set at the inlet. The average static pressure (determined by the expansion ratio) and 5% pressure profile blend are given at the outlet. The sand grain roughness and adiabatic conditions are specified at the hub, the shroud, and the blade, respectively. In order to avoid reverse flow, two extensions at a distance equivalent to approximately 25% of the stator chord are added in front of and behind the stator passage domain [19]. As only one stator passage is simulated, the periodic boundary condition is set at the interface.

The numerical method is validated against the detailed experimental data for the gas radial rotor [33] and axial turbine [34] presented by NASA Lewis Research Center. The apparatus in their investigations consists of the turbine, an inlet and exhaust system with flow control valves, and a dynamometer to control the speed, absorb the output power, and measure turbine torque. The dry pressurized air is firstly ducted through a flow meter and then through the control valves, by which the inlet pressure is reduced and controlled. The air with suitable pressure is then directed to an air heater and then enters the turbine test section. The turbine exhaust pressure is set by the use of the other control valves. Both two experiments were conducted under the cold-air conditions. According to the data given in the reports, the boundary conditions are given at the inlet and outlet, respectively. Both the computational meshes and validation results are shown in Fig. 4, which

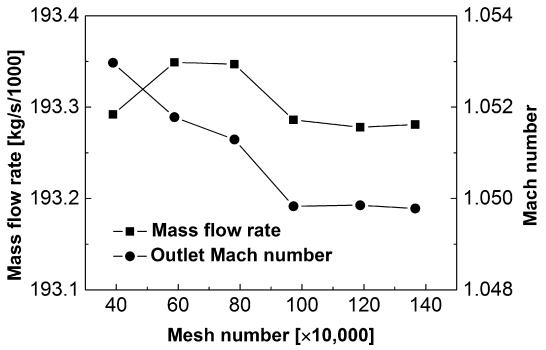

Fig. 3. Results of the mesh independence analysis.

indicate that the feasibility of the proposed numerical method for the turbine machine.

As shown in Fig. 5, the organic vapor expands from state 0 to state 1s under the ideal condition. Due to the flow loss, the state of working fluid at the stator outlet changes from 1s to 1. Since the inlet velocity is quite low, it is assumed to be zero and the total enthalpy is equal to the static enthalpy at the stator inlet. We also assume that there is no heat emission to the environment due to the high speed flow in the stator.

Based on the above description, the isentropic total enthalpy at the stator outlet is calculated by:

$$h_{1s}^{*} = h_{1s} + \frac{1}{2}c_1^2 \tag{8}$$

where the subscripts 1 and 1s represent the stator outlet and the isentropic outlet, h and c are the enthalpy and the velocity, respectively.

The total enthalpies at the stator inlet and outlet are equal:

$$h_0^{*} = h_1^{*} = h_1 + \frac{1}{2}c_1^2 = h_{1s} + \frac{1}{2}c_{1s}^2 \tag{9}$$

where the subscript 0 represents the stator inlet.

According to Eqs. (8) and (9), the outlet isentropic velocity can be given by:

$$c_{1s} = \sqrt{2(h_0^{*} - h_{1s}^{*}) + c_1^2} \tag{10}$$

The velocity coefficient can be therefore obtained from the CFD results:

$$\varphi = \frac{c_1}{\sqrt{2(h_0^{*} - h_{1s}^{*}) + c_1^2}} \tag{11}$$

In the preliminary 1-D design, NASA Lewis Research Center proposed the loss model to determine the 3-D viscous loss in the stator [35], which are shown as follows:

$$\varphi = \sqrt{1 - \zeta_n} \tag{12}$$

$$\zeta_n = \frac{\mathrm{EC}\left(\frac{\theta_{tot}}{l}\right)_{ref}\left(\frac{Re}{Re_{ref}}\right)^{-0.2}\left(\frac{l}{s}\right)\left(\frac{A_{3D}}{A_{2D}}\right)}{\cos\gamma - \frac{t}{s} - \mathrm{HC}\left(\frac{\theta_{tot}}{l}\right)_{ref}\left(\frac{Re}{Re_{ref}}\right)^{-0.2}\left(\frac{l}{s}\right)} \tag{13}$$

where E is the energy factor, C is the loss coefficient multiplier, θ is the momentum thickness, l is the surface length (leading edge to trailing edge), Re is the Reynolds number, s is blade spacing at blade-row exit, A is the area, γ is the flow angle from the through-flow direction, t is the trailing-edge thickness, H is the form factor, subscript tot represents total, and subscript ref represents reference. The detailed explanation of each parameter can be found in Appendix.

According to the corresponding equation, γ directly relates to the stator outlet blade angle α; l can be calculated by the chord b; blade height d can influence the values of Re, t, and A_{3D}/A_{2D}; both E and H are partly determined by the outlet Mach number, which has positive correlation with the expansion ratio π. Several key geometric parameters of stator are shown in Fig. 6. In addition, the surface roughness R_x also affects the flow loss in the stator but is not considered in the prediction model. As a result, five affecting parameters, outlet blade angle, solidity (b/s), blade height, expansion ratio, and surface roughness, are selected to investigate the effects on the stator velocity coefficient. As shown in Fig. 1, the main input dimensions include the chord, outlet blade angle, blade height, and blade spacing. The expansion ratio and surface roughness are set as the boundary conditions. Table 3 lists the ranges of the considered variables.

Fig. 7 shows the comparison of the velocity coefficients for the different cases obtained from the mentioned 1-D prediction model and the 3-D numerical simulation. It can be found that both results for the stator with smooth wall show good agreement with a maximum deviation around 1.5%, and the stator velocity coefficients for smooth walls are mostly within the recommended range of 0.92–0.98 [32]. By contrast, the introduction of the surface roughness factor results in obviously lower stator velocity coefficients, especially for the stator with higher surface roughness. It causes great deviation from the data of the 1-D prediction model, in which the effect of surface roughness is not taken into account. Therefore, it is necessary to further investigate the effects of the surface roughness and other variables (α, b/s, d, π) under the rough wall condition on the velocity coefficient for the stator using organic vapor.

3. Parametric analysis of key inputs

The analysis of influence factors for the stator velocity coefficient is conducted in this section. When considering the impact of single parameter, other geometric parameters are fixed as follows: d = 5 mm, R_x = 30 μm, α = 15°, and b/s = 1.516. Firstly, the variation of the velocity coefficient with the expansion ratio is shown in Fig. 8. Under the different conditions of blade height, surface roughness, outlet blade angle, and solidity, the velocity coefficient slightly increases along with the increasing expansion ratio, but its increase degree is limited. Except for the stator with smaller blade height (≤3 mm), the velocity coefficient varies by less than 0.01 within the considered range of expansion ratio. It illustrates that the effect of expansion ratio on the velocity coefficient can be negligible. Therefore, expansion ratio is not considered as one of the key influence factors and its value is fixed at 2.6 for further study.

Fig. 9 shows the velocity coefficient depends on the surface roughness and other influence factors (d, α, and b/s). Overall velocity coefficient decreases with the increase of the surface roughness and solidity and the decrease of the blade height and outlet blade angle. Due to the change of the relative height of the viscous sub-

Table 2
Fluid properties of R123.

	P_{cr} [kPa]	T_{cr} [K]	M [kg/kmol]	$T_{boiling}$ [K]	ω	ODP	GWP
R123	3661.8	456.83	152.93	300.97	0.28192	0.012	120

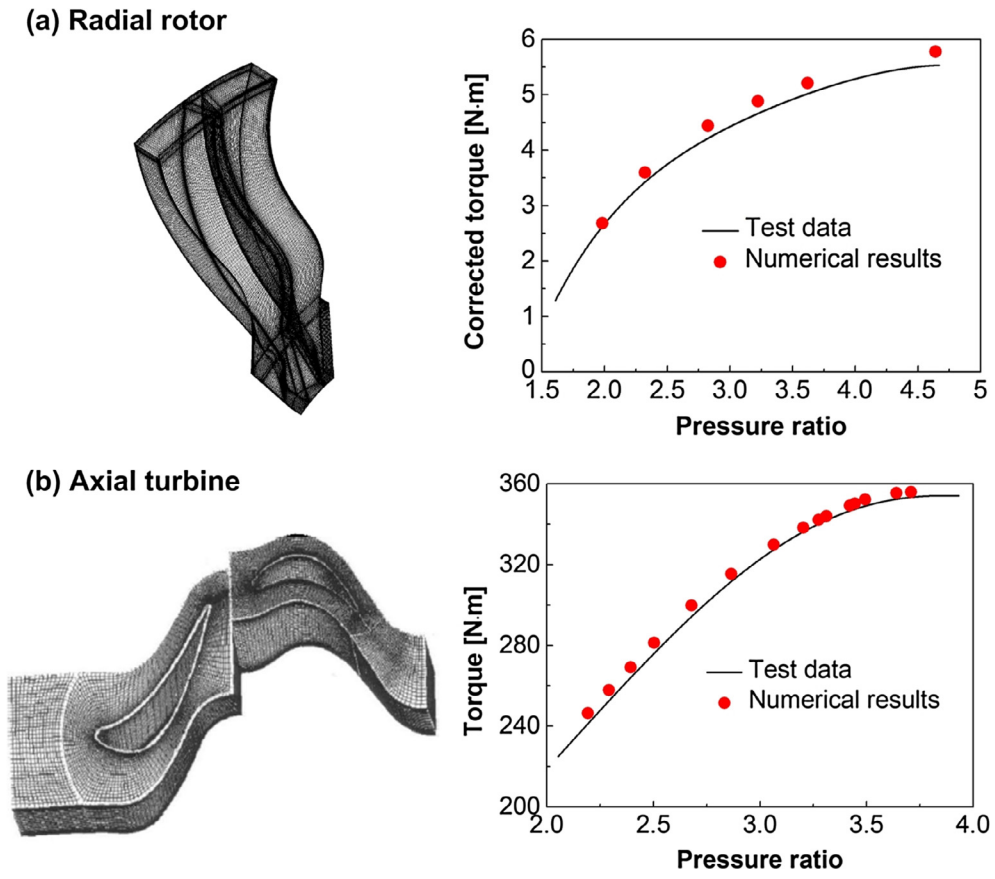

Fig. 4. Comparisons between experimental and numerical results.

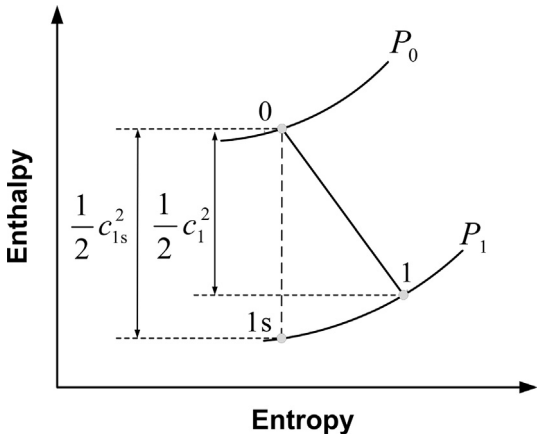

Fig. 5. Enthalpy-entropy diagram of the flow in the stator.

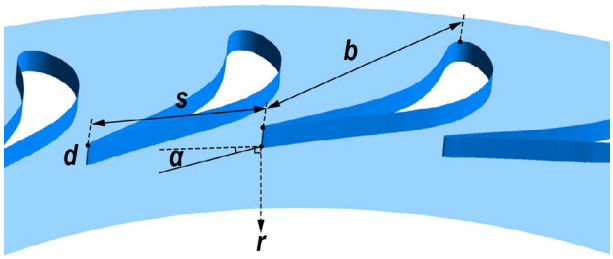

Fig. 6. Geometry schematic of stator with key parameters.

Table 3
The ranges of the considered influence parameters.

Parameter	Value	Reference
Outlet blade angle, α (°)	12–18	[26,32]
Solidity, b/s	1.3–1.8	[32]
Blade height, d (mm)	2–8	[19,32]
Expansion ratio, π	2–3	[19,26]
Surface roughness, R_x (μm)	0–60	–

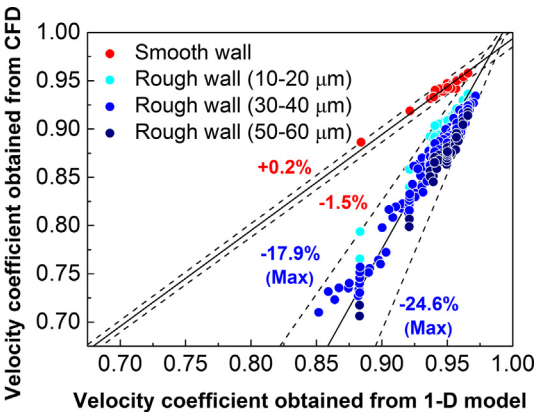

Fig. 7. Comparison of velocity coefficients obtained from Eq. (13) and CFD simulation.

layer, the effect of blade height on the velocity coefficient is more significant than the surface roughness (Fig. 9(a)). While the effects

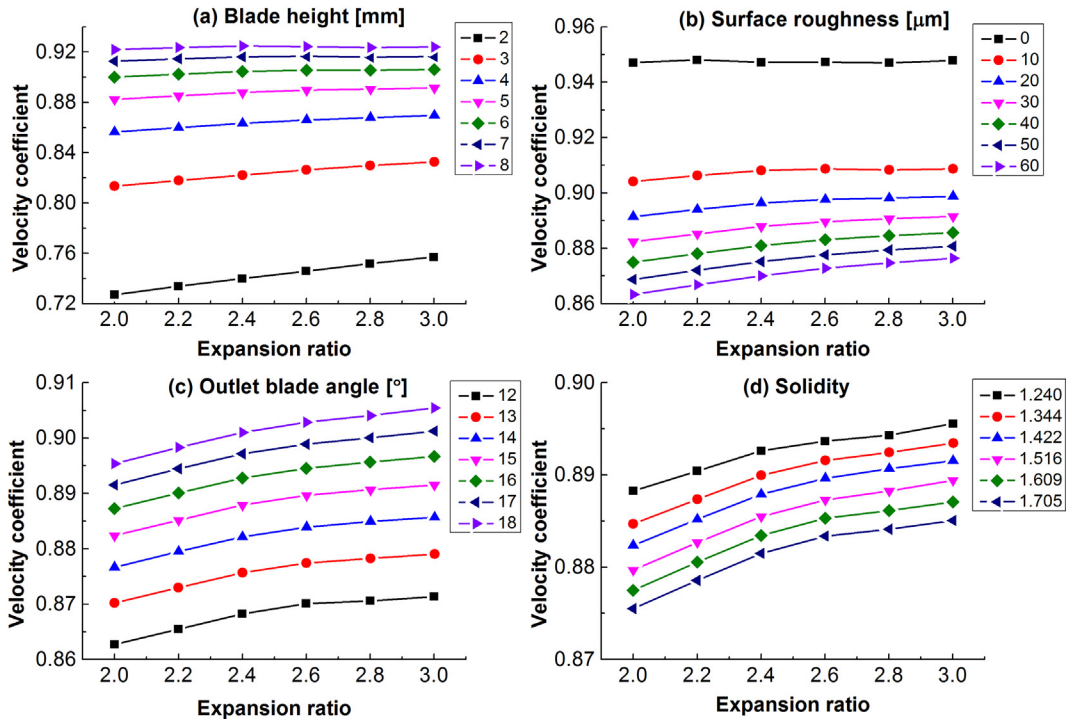

Fig. 8. Velocity coefficient versus expansion ratio.

of the outlet blade angle and solidity are relatively small (Fig. 9(b) and (c)). The velocity coefficient increases from 0.746 to 0.924 when the blade height changes from 2 mm to 8 mm at the surface roughness of 30 μm, and it varies from 0.943 to 0.873 when the surface roughness changes from 0 μm to 60 μm at the blade height of 5 mm. By comparison, the velocity coefficients only change 0.0327 and 0.0103 within the considered ranges of outlet blade angle and solidity. Additionally, the effects of blade height, outlet blade angle, and solidity on the velocity coefficient are simultaneously influenced by the surface roughness. For the stator with smooth wall, above variables show relatively less influence on the velocity coefficient than that under the rough wall condition.

Fig. 10 further illustrates the variation of the velocity coefficient with the blade height, outlet blade angle, and solidity. It can be found that there exits coupling effect of blade height and outlet blade angle on the velocity coefficient: as the blade height increases, the influence of outlet blade angle is gradually decreased. By contrast, the effect of solidity on the velocity coefficient basically shows minimal or no dependence on the blade height and the outlet blade angle. It also shows that the outlet blade angle has more significant impact on the velocity coefficient than the solidity. Generally, blade height shows the most significant influence on the stator velocity coefficient, followed by the surface roughness, outlet blade angle, solidity, and expansion ratio.

4. Prediction model modification

Due to the notable deviation between the results from 1-D model and CFD simulation for the stator with rough wall, the 1-D predication model is modified by introducing surface roughness factor. In the original equation, E is the energy factor determined by approximating the velocity profile exponent to be 0.2. Since the surface roughness directly affects the velocity distribution, E should be adjusted along with the surface roughness. According to 358 numerical experiments, a series of data fittings with various types of correction terms were conducted in MATLAB R2013a in order to find the lowest error bands. The results show that adding the product term of energy factor in the form of $(a + bR_x)^c$ can obtain the most accurate results, and the calibrated expression for the energy factor is expressed as follows:

$$E_f = (1.640 + 1.634R_x)^{0.187}E \tag{14}$$

Accordingly the original prediction model can be modified:

$$\zeta_{nf} = \frac{(1.640 + 1.634R_x)^{0.187}EC\left(\frac{\theta_{tot}}{l}\right)_{ref}\left(\frac{Re}{Re_{ref}}\right)^{-0.2}\left(\frac{l}{s}\right)\left(\frac{A_{3D}}{A_{2D}}\right)}{\cos\gamma - \frac{t}{s} - HC\left(\frac{\theta_{tot}}{l}\right)_{ref}\left(\frac{Re}{Re_{ref}}\right)^{-0.2}\left(\frac{l}{s}\right)} \tag{15}$$

As shown in Fig. 11, the stator velocity coefficients obtained from the modified model show better agreement with that from CFD simulation, with a deviation range from −3.5% to +2.5%. This illustrates that the modified model can make a good prediction of the velocity coefficient for the stator with R123 as working fluid.

Fig. 12 explores the applicability of the modified model into different inlet condition and working fluid. Here, all the involved stators were simulated at the expansion ratio of 2.6 with the same geometrical structure, in which the height is 5 mm, the outlet blade angle is 15°, and the solidity is 1.561. The inlet temperature is selected in the range of 380–410 K, and the inlet pressure is slightly low than the corresponding saturation pressure. From the simulation results, the stator velocity coefficient decreases with increasing inlet temperature. However, similar trend is not shown in the 1-D prediction results for the stator using R123. For another frequently selected ORC working fluid R245fa, two results obtained from 1-D model and CFD simulation have the same trend. In general, the velocity coefficients determined by modified model match quite well with the numerical results. The maximum deviations are 1.19% for R123 at the inlet conditions of 410 K and 1500 kPa and 1.81% for R245fa at 400 K and 2000 kPa, respectively. The average deviations for two refrigerants are only 0.44% and 1.00%, reflecting the prediction capabilities of the modified model for the stator velocity coefficients among different operating conditions and refrigerants.

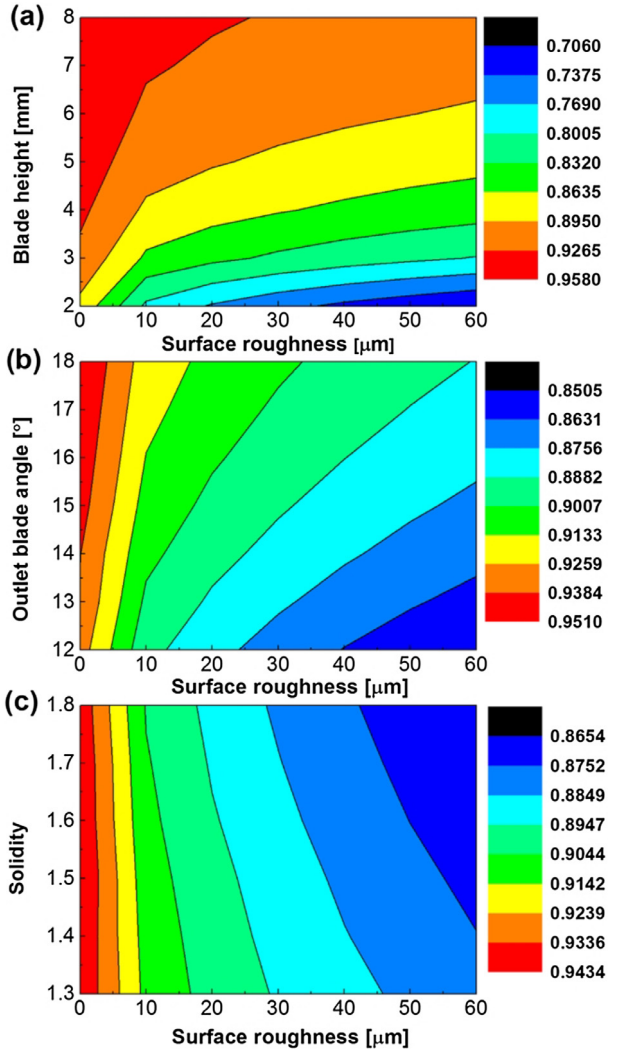

Fig. 9. Velocity coefficient versus surface roughness and other factors.

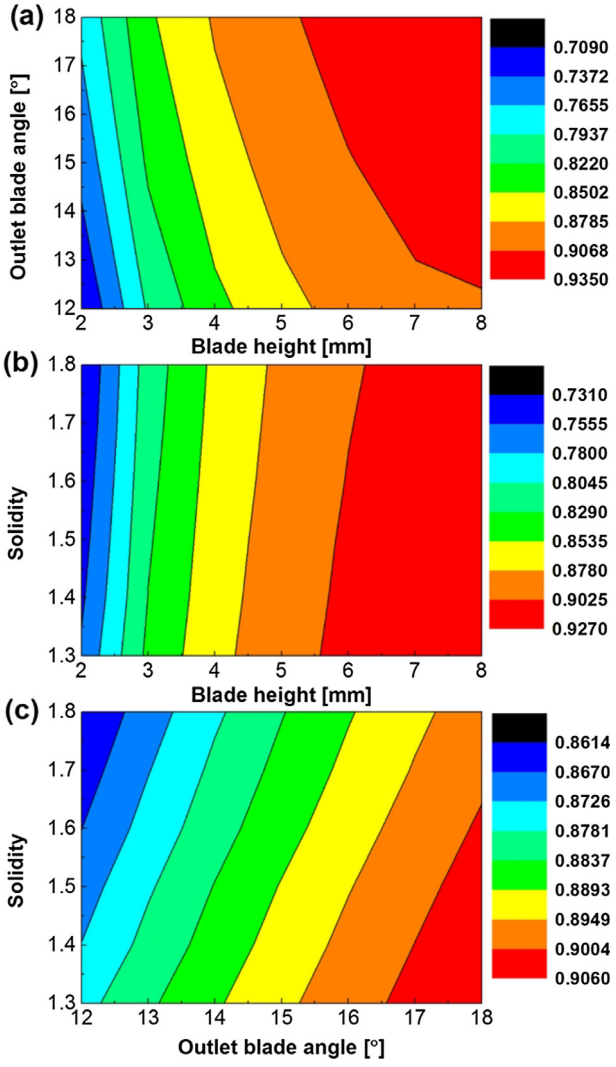

Fig. 10. Velocity coefficient versus blade height, outlet blade angle, and solidity.

Why is the modified model developed from the data of R123 also applicable for other refrigerants? One possible reason lies in the effect of the high Reynolds number for the stator using refrigerant vapor. As shown in Fig. 13, similar to the hydraulic roughness, aerodynamic roughness is divided into aerodynamically smooth region, transitional region, and completely rough region. In the aerodynamically smooth region, the lower Reynolds number brings the thicker flow boundary layer, leading to little influence of surface roughness on the flow resistance. As such, the flow resistance is only related to the Reynolds number. The stator loss model proposed by NASA was obtained based on the gas turbine with relatively lower Reynolds number in the stator, which explains that there is no surface roughness related item in the loss model for the gas radial turbine stator. As the Reynolds number increases, the boundary layer becomes thinner and the flow enters the aerodynamically transitional region, where the flow resistance depends both on the Reynolds number and the surface roughness. With the further increasing of the Reynolds number, the effect of boundary layer can be neglected in the aerodynamically rough region and the flow resistance is relevant only to the surface roughness. Regarding the stator using R123, the expansion ratio, which is directly related to the Reynolds number, has little effect on the velocity coefficient (Fig. 8). It tells that the Reynolds number is so enough that it is basically irrelevant to the friction loss, and therefore the surface

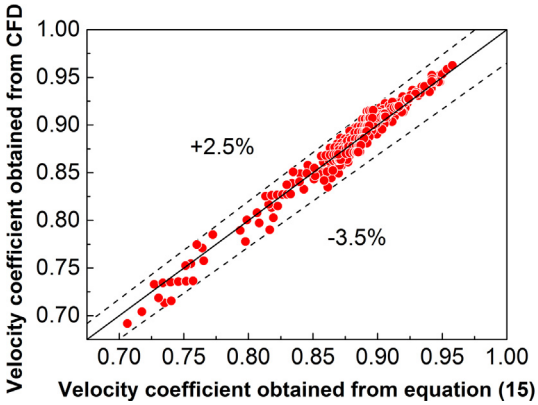

Fig. 11. Comparison of stator velocity coefficients obtained from modified equation and CFD simulation.

roughness is the only influencing factor. According to the numerical results of the velocity coefficients for the stators with R245 as working fluid, the flow resistance is also partly determined by the surface roughness. Except for the friction loss, the results for the stator with smooth surface in Fig. 7 illustrate that the effects

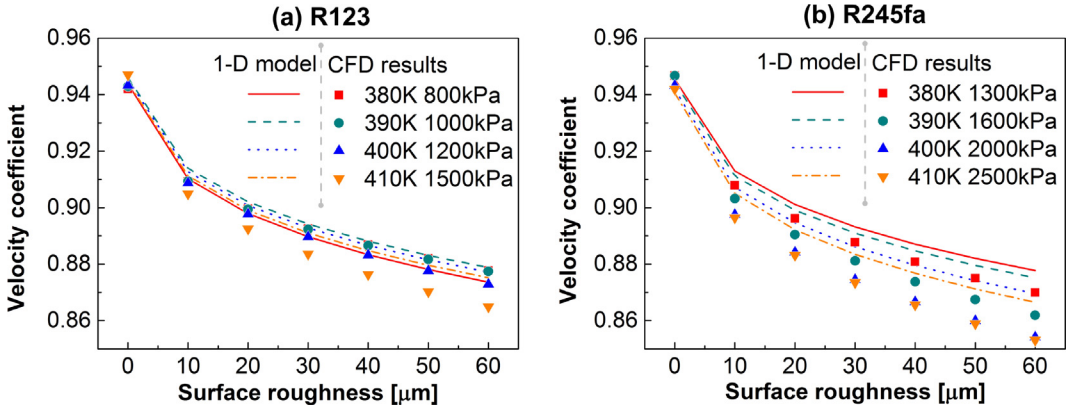

Fig. 12. Comparisons of velocity coefficients obtained from original and modified models for stators with R123 (a) and R245fa (b).

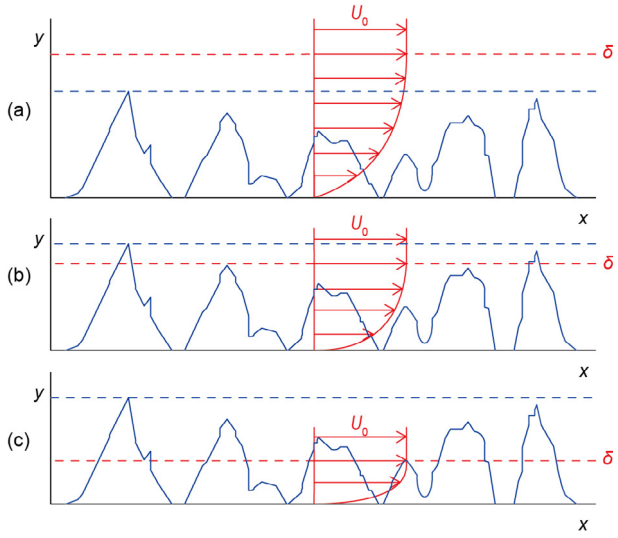

Fig. 13. Diagram of the aerodynamic roughness: (a) aerodynamically smooth region, (b) transitional region, (c) completely rough region.

of other factors on the velocity coefficients are the same between using refrigerant vapor and compressed air. Therefore, adding a product term considering surface roughness in the modified model could be feasible for estimating the velocity coefficient for the stators with various refrigerant working fluids.

The following briefly explains the effect of using the proposed modified model on the ORC performance. As stated before, velocity coefficient is a generally adopted parameter to determine the stator loss. Due to the decrease of the speed in the stator, part of the kinetic energy is converted into heat, which can be expressed as follows:

$$q_s = \frac{1}{2}c_{1s}^2 - \frac{1}{2}c_1^2 = \frac{1}{2}(1-\varphi^2)c_{1s}^2 = (1-\varphi^2)h_{1s} \tag{16}$$

So the relative energy loss in the stator is obtained:

$$\xi_s = q_s/h_{1s} = 1-\varphi^2 \tag{17}$$

Take the stator with $\alpha = 15°$, $b/s = 1.516$, $d = 5$ mm, $R_x = 30$ mm, and $\pi = 2.6$ as an example, its velocity coefficient determined by the 1-D model from NASA is 0.950, which is consistent with the previous study [12]. However, the velocity coefficient from the modified model is 0.893, very close to the value of 0.890 obtained from the CFD method. Using two prediction models, the relative energy losses are 0.0974 and 0.203, respectively. It can be found that the relative energy loss is doubled when using the modified model, resulting in up to a 10% decrease in the turbine isentropic efficiency. Therefore, the cycle thermal efficiency can be reduced by about 10%.

5. Conclusion

This work presents the numerical analysis of the stator velocity coefficient for the radial ORC turbine using R123 as working fluid. The effects of outlet blade angle, solidity, blade height, expansion ratio, and surface roughness on the velocity coefficient are investigated for the transonic blade profile TC-4P. By fitting the numerical results, a 1-D prediction model is modified with a term related to the surface roughness, and its applicability to other inlet parameters and refrigerants is preliminarily investigated as well. Major conclusions of this paper are drawn as follows:

Among the considered factors, blade height and surface roughness are the key parameters to determine the stator velocity coefficient, whereas the expansion ratio has negligible impact on the velocity coefficient. The velocity coefficient for the stator with smooth wall can be determined through the existing semi-empirical formula, but which is not effective to predict the stator velocity coefficient under the rough wall condition. The modified model accounting for the influence of the surface roughness greatly improves the predication accuracy. The results obtained from the modified model show better agreement with that from numerical simulations, with a deviation range from −3.5% to +2.5% within the investigated parameter range. Due to the high Reynolds number and resulting thin flow boundary layer, the proposed model fitted by the stator with R123 is also applicable for the stator using R245fa within a wide range of inlet condition, indicating the potentially wide application of the modified model.

Generally, the modified model proposed in this study significantly improves the preliminary design accuracy of the radial turbine in low-grade ORC system. Further work may be required to improve the modified model, such as introducing more data from the stators with different refrigerants and boundary conditions, and conducting the experimental testing for the stator velocity coefficient in the radial ORC turbine.

Acknowledgement

B.D. thanks the funding supporting from the "Zhuoyue" post-doctoral program at Beihang University. The authors acknowledge the editor Professor Christos Markides for handling the manuscript and the reviewers for their constructive comments that have significantly improved the manuscript.

Appendix A

Following explanations are developed and summarized by Glassman [35].

In Eq. (7), the energy factor E and form factor H, which present the characteristics of boundary layer flow, can be calculated as follows:

$$E = \frac{2\left(\frac{1}{1.92} + \frac{Q}{3.2} + \frac{Q^2}{4.8} + \frac{Q^3}{6.72}\right)}{\frac{1}{1.68} + \frac{Q}{2.88} + \frac{Q^2}{4.4} + \frac{Q^3}{6.24}} \tag{A.1}$$

$$H = \frac{\frac{1}{1.2} + \frac{3Q}{1.6} + \frac{5Q^2}{2.0} + \frac{7Q^3}{2.4} + \frac{9Q^4}{2.8}}{\frac{1}{1.68} + \frac{Q}{2.88} + \frac{Q^2}{4.4} + \frac{Q^3}{6.24}} \tag{A.2}$$

$$Q = \frac{k-1}{k+1}\left(\frac{c_1}{c_{cr1}}\right)^2 \tag{A.3}$$

where k: specific heat ratio (c_p/c_v); c: absolute velocity (m/s); subscript cr: critical condition; subscript 1: outlet.

Regarding the stator, when the loss coefficient multiplier C is set to 1,

$$\left(\frac{\theta_{tot}}{l \cdot Re^{-0.2}}\right)_{ref} = 0.03734 \tag{A.4}$$

Reynolds number Re can be obtained by:

$$Re = \frac{\rho_1 c_1 b}{\mu_1} = \frac{m}{\pi(d/b)\mu_1 d_1 \cos(90 - \alpha_1)} \tag{A.5}$$

where ρ: density (kg/m^3); μ: dynamic viscosity (Pa·s); m: mass flow rate (kg/s); d_1: outlet diameter (m).

For the surface length to blade spacing ratio l/s:

$$\frac{l}{s} = \frac{b}{s}\cdot\frac{l}{b} = \frac{b}{s}\cdot\frac{\pi\theta_{cam}}{360\sin\frac{\theta_{cam}}{2}} \tag{A.6}$$

where θ_{cam} is the camber angle with the following expression:

$$\theta_{cam} = \alpha_0 - \alpha_1 - \cos^{-1}\left(\frac{r_0^2 + r_1^2 - b^2}{2r_0 r_1}\right) \tag{A.7}$$

where r: radius (m); subscript 0: inlet.

The 3-D to 2-D area ratio A_{3D}/A_{2D} can be calculated by:

$$\frac{A_{3D}}{A_{2D}} = \frac{A_b + A_w}{A_b} = 1 + \frac{r_0^2 - r_1^2}{2r_1 l/sd} \tag{A.8}$$

where subscript b: blade; subscript w: endwall.

The trailing-edge thickness t is set as 5% of the blade height yields

$$\frac{t}{s} = 0.05\frac{d}{s} \tag{A.9}$$

References

[1] N. Kazemi, F. Samadi, Thermodynamic, economic and thermo-economic optimization of a new proposed organic Rankine cycle for energy production from geothermal resources, Energy Convers. Manage. 121 (2016) 391–401.

[2] A. Borsukiewicz-Gozdur, S. Wisniewski, S. Mocarski, M. Bankowski, ORC power plant for electricity production from forest and agriculture biomass, Energy Convers. Manage. 87 (2014) 1180–1185.

[3] A. Daabo, S. Mahmoud, R. Al-Dadah, A. Jubori, A. Ennil, Numerical analysis of small scale axial and radial turbines for solar powered Brayton cycle application, Appl. Therm. Eng. 120 (2017) 672–693.

[4] D. Budisulistyo, S. Krumdieck, A novel design methodology for waste heat recovery systems using organic Rankine cycle, Energy Convers. Manage. 142 (2017) 1–12.

[5] B. Dong, G. Xu, Y. Cai, H. Li, Analysis of zeotropic mixtures used in high-temperature Organic Rankine cycle, Energy Convers. Manage. 84 (2014) 253–260.

[6] P. Garg, G.M. Karthik, P. Kumar, P. Kumar, Development of a generic tool to design scroll expanders for ORC applications, Appl. Therm. Eng. 109 (2016) 878–888.

[7] A. Giuffrida, Improving the semi-empirical modelling of a single-screw expander for small organic Rankine cycles, Appl. Energy 193 (2017) 356–368.

[8] P. Kolasinski, P. Blasiak, J. Rak, Experimental and numerical analyses on the rotary vane expander operating conditions in a micro organic Rankine cycle system, Energies 9 (2016) 15.

[9] J. Bao, L. Zhao, A review of working fluid and expander selections for organic Rankine cycle, Renew. Sustain. Energy Rev. 24 (2013) 325–342.

[10] D. Fiaschi, G. Manfrida, F. Maraschiello, Design and performance prediction of radial ORC turboexpanders, Appl. Energy 138 (2015) 517–532.

[11] K. Rahbar, S. Mahmoud, R.K. Al-Dadah, N. Moazami, Parametric analysis and optimization of a small-scale radial turbine for Organic Rankine Cycle, Energy 83 (2015) 696–711.

[12] J. Song, C.W. Gu, X. Ren, Influence of the radial-inflow turbine efficiency prediction on the design and analysis of the Organic Rankine Cycle (ORC) system, Energy Convers. Manage. 123 (2016) 308–316.

[13] L. Pan, H. Wang, Improved analysis of Organic Rankine Cycle based on radial flow turbine, Appl. Therm. Eng. 61 (2013) 606–615.

[14] A. Pezzuolo, A. Benato, A. Stoppato, A. Mirandola, The ORC-PD: a versatile tool for fluid selection and Organic Rankine Cycle unit design, Energy 102 (2016) 605–620.

[15] J. Hoffren, T. Talonpoika, J. Larjola, T. Siikonen, Numerical simulation of real-gas flow in a supersonic turbine nozzle ring, J. Eng. Gas Turbines Power 124 (2002) 395–403.

[16] J. Harinck, T. Turunen-Saaresti, P. Colonna, S. Rebay, J. van Buijtenen, Computational study of a high-expansion ratio radial organic rankine cycle turbine stator, J. Eng. Gas Turbines Power 132 (2010) 054501.

[17] P. Boncinelli, F. Rubechini, A. Arnone, M. Cecconi, C. Cortese, Real gas effects in turbomachinery flows: a computational fluid dynamics model for fast computations, J. Turbomach. 126 (2004) 268–276.

[18] J. Harinck, D. Pasquale, R. Pecnik, J. van Buijtenen, P. Colonna, Performance improvement of a radial organic Rankine cycle turbine by means of automated computational fluid dynamic design, Proc. Inst. Mech. Eng., Part A: J. Power Energy 227 (2013) 637–645.

[19] E. Sauret, Y. Gu, Three-dimensional off-design numerical analysis of an organic Rankine cycle radial-inflow turbine, Appl. Energy 135 (2014) 202–211.

[20] Y. Li, X.-D. Ren, Investigation of the organic Rankine cycle (ORC) system and the radial-inflow turbine design, Appl. Therm. Eng. 96 (2016) 547–554.

[21] Y. Li, X.S. Li, X. Ren, Aerodynamic optimization of a high-expansion ratio organic radial-inflow turbine, J. Mech. Sci. Technol. 30 (2016) 5485–5490.

[22] A. Al Jubori, R.K. Al-Dadah, S. Mahmoud, Development of micro-scale radial inflow turbine for Organic Rankine Cycle, in: 2016 International Conference for Students on Applied Engineering (Icsae), 2016, pp. 164–169.

[23] A.A. Jubori, A. Daabo, R.K. Al-Dadah, S. Mahmoud, A.B. Ennil, Development of micro-scale axial and radial turbines for low-temperature heat source driven organic Rankine cycle, Energy Convers. Manage. 130 (2016) 141–155.

[24] D. Fiaschi, G. Innocenti, G. Manfrida, F. Maraschiello, Design of micro radial turboexpanders for ORC power cycles: From OD to 3D, Appl. Therm. Eng. 99 (2016) 402–410.

[25] F. Hamdi, J. Seo, S. Han, Numerical investigation of an Organic Rankine cycle radial inflow two-stage turbine, J. Mech. Sci. Technol. 31 (2017) 1721–1728.

[26] B. Dong, G. Xu, X. Luo, L. Zhuang, Y. Quan, Analysis of the supercritical Organic Rankine Cycle and the radial turbine design for high temperature applications, Appl. Therm. Eng. 123 (2017) 1523–1530.

[27] S.H. Kang, Design and experimental study of ORC (organic Rankine cycle) and radial turbine using R245fa working fluid, Energy 41 (2012) 514–524.

[28] S.H. Kang, Design and preliminary tests of ORC (organic Rankine cycle) with two-stage radial turbine, Energy 96 (2016) 142–154.

[29] L. Li, Y.T. Ge, X. Luo, S.A. Tassou, Experimental investigations into power generation with low grade waste heat and R245fa Organic Rankine Cycles (ORCs), Appl. Therm. Eng. 115 (2017) 815–824.

[30] N. Inoue, A. Kaneko, H. Watanabe, T. Uchimura, K. Irie, Asme, Development of Electric Power Generation Unit Driven by Waste Heat: (Study on Working Fluids and Expansion Turbines), Amer Soc Mechanical Engineers, New York, 2007.

[31] L. Guillaume, A. Legros, A. Desideri, V. Lemort, Performance of a radial-inflow turbine integrated in an ORC system and designed for a WHR on truck application: an experimental comparison between R245fa and R1233zd, Appl. Energy 186 (2017) 408–422.

[32] G. Ji, Turboexpander, China Machine Press, 1989.

[33] K.L. Mclallin, J.E. Haas, Experimental Performance and Analysis of 15.04-centimeter-tip-diameter, Radial-inflow turbine with Work Factor of 1.126 and Thick Blading, 1980.

[34] T.P. Moffitt, E.M. Szanca, W.J. Whitney, F.P. Behning, Design and Cold-air Test of Single-stage Uncooled Turbine with High Work Output, 1980.

[35] A.J. Glassman, Computer Program for Design Analysis of Radial-inflow Turbines, 1976.